A head-to-toe dimerization has physiological relevance for ligand-induced inactivation of protein tyrosine receptor type Z

Received for publication, February 5, 2019, and in revised form, August 7, 2019 Published, Papers in Press, August 15, 2019, DOI 10.1074/jbc.RA119.007878

Akihiro Fujikawa[‡], Hajime Sugawara[§1], Naomi Tanga[‡¶], Kentaro Ishii[‖], Kazuya Kuboyama[‡2], Susumu Uchiyama[‖], Ryoko Suzuki[‡], and Masaharu Noda[‡¶‡‡3]**

*From the [‡]Division of Molecular Neurobiology, National Institute for Basic Biology (NIBB), 5-1 Higashiyama, Myodaiji-cho, Okazaki, Aichi 444-8787, Japan, [§]Asubio Pharma Co., Ltd., 6-4-3 Minatojima-Minamimachi, Chuo-ku, Kobe, Hyogo 650-0047, Japan, the [¶]School of Life Science, Graduate University for Advanced Studies (SOKENDAI), 5-1 Higashiyama, Myodaiji-cho, Okazaki, Aichi 444-8787, Japan, the [‖]Exploratory Research Center on Life and Living Systems (ExCELLS), National Institutes of Natural Sciences, 5-1 Higashiyama, Myodaiji-cho, Okazaki 444-8787, Japan, the **Department of Biotechnology, Graduate School of Engineering, Osaka University, 2-1 Yamadaoka, Suita, Osaka 565-0871, Japan, and the [‡‡]Institute of Innovative Research, Tokyo Institute of Technology, 4529 Nagatsuta-cho, Midori-ku, Yokohama, Kanagawa 226-8503, Japan*

Edited by Alex Toker

Protein-tyrosine phosphatase (PTPase) receptor type Z (PTPRZ) has two receptor isoforms, PTPRZ-A and -B, containing tandem intracellular PTP-D1 and -D2 domains, with only D1 being active. Pleiotrophin (PTN) binding to the extracellular PTPRZ region leads to inactivation of its PTPase activity, thereby facilitating oligodendrocyte precursor cell (OPC) differentiation and myelination in the central nervous system. However, the mechanisms responsible for PTN-induced PTPRZ inactivation remain unclear. We herein report that the crystal structure of the intracellular region of PTPRZ (PTPRZ-ICR) shows a "head-to-toe"-type dimer conformation, with D2 masking the catalytic site of D1. MS analyses revealed that PTPRZ-ICR proteins remain in monomer-dimer equilibrium in aqueous solution and that a substrate-derived inhibitory peptide or competitive inhibitor (SCB4380) specifically bind to the monomer form in a 1:1 ratio. A D2 deletion (ΔD2) or dimer interface mutation (DDKK) disrupted dimer formation, but SCB4380 binding was maintained. Similar to WT PTPRZ-B, monomer-biased PTPRZ-B-ΔD2 and PTPRZ-B-DDKK variants efficiently dephosphorylated p190RhoGAP at Tyr-1105 when co-expressed in BHK-21 cells. The catalytic activities of these variants were not suppressed by PTN treatment, but were inhibited by the cell-permeable PTPase inhibitor NAZ2329. Of note, the PTN treatment did not enhance OPC differentiation in primary cultured glial cells from ΔD2 or PTPase-inactive PTPRZ-B (CS) mutant knock-in mice. Our results thus indicate that PTN-induced PTPRZ inactivation results from dimer formation of the intracellular tandem PTP domains in a head-to-toe configuration, which is physiologically relevant to the control of OPC differentiation *in vivo*.

The tyrosine phosphorylation of cellular proteins in higher eukaryotes serves as an important signal transduction system in various cellular events, including cell proliferation, migration, and differentiation (1). This phosphorylation is reversibly controlled by protein-tyrosine kinases (PTKs)[4] and protein-tyrosine phosphatases (PTPs). The regulatory mechanisms of receptor PTKs (RPTKs) have been extensively examined; the ligand-induced dimerization of RPTKs leads to the trans-phosphorylation of key tyrosine residues in the activation loop, resulting in the full activation of its catalytic activity (2).

In contrast to RPTKs, the dimerization-induced inactivation model of receptor-type PTP (RPTP) activity has remained controversial. RPTPs have a similar structure comprising a unique extracellular domain, single transmembrane domain, and one or two intracellular PTP domains. In the latter case with two PTP domains, the membrane proximal PTP domain (D1) exhibits PTP activity, whereas the distal PTP domain (D2) has little or no catalytic activity (3). In the late 1990s, the dimerization-induced inactivation mechanism of RPTP was initially suggested by structural studies on the D1 of PTPRA/PTPα (4, 5). The crystal structure of PTPRA-D1 indicated a dimeric assembly in which the N-terminal helix-turn-helix wedge motif occluded the active site in the catalytic domain of the interacting counterpart. However, subsequent structural studies on the cytoplasmic tandem D1D2 segments of PTPRF/LAR (6), PTPRC/CD45 (7), and PTPRG/PTPγ (8) showed that the ori-

This work was supported in part by Japan Society for the Promotion of Science (JSPS) KAKENHI Grants 17K07069 and 26110722 (to A. F.), 17K07355 (to K. K.), and 16209008 and 08458187 (to M. N.). The authors declare that they have no conflicts of interest with the contents of this article.

This article contains Tables S1 and S2 and Figs. S1–S4.

The atomic coordinates and structure factors (code 6J6U) have been deposited in the Protein Data Bank (http://wwpdb.org/).

[1] Present address: Shinagawa R&D Center, Daiichi-Sankyo Co., Ltd., 1-2-58 Hiromachi, Shinagawa-ku, Tokyo 140-8710, Japan.

[2] Present address: Dept. of Neuropharmacology, Kagawa School of Pharmaceutical Sciences, Tokushima Bunri University, 1314-1 Shido, Sanuki, Kagawa 769-2193, Japan.

[3] To whom correspondence should be addressed: Institute of Innovative Research (IIR), Tokyo Institute of Technology, S2 4259 Nagatsuta-cho, Midori-ku, Yokohama, Kanagawa 226-8503, Japan. Tel.: 81-45-924-5537; E-mail: noda.m.ae@m.titech.ac.jp.

[4] The abbreviations used are: PTK, protein-tyrosine kinases; PTP, protein-tyrosine phosphatase; PTPRZ, protein-tyrosine phosphatase receptor type Z; CS, chondroitin sulfate; PTN, pleiotrophin; OPC, oligodendrocyte precursor cell; GAP, GTPase-activating protein; RPTP, receptor-type protein-tyrosine phosphatase; MBP, myelin basic protein; NG2, neural/glial antigen 2 chondroitin sulfate; chABC, chondroitinase ABC; bistris propane, 1,3-bis[tris(hydroxymethyl)methylamino]propane; BHK, baby hamster kidney; CAH, carbonic anhydrase; PDB, Protein Data Bank; DMEM, Dulbecco's modified Eagle's medium; TBS, Tris-buffered saline; DAPI, 4′,6-diamidino-2-phenylindole.

entations of the D1 and D2 domains were highly conserved and incompatible with the "inhibitory wedge model" due to a steric clash. In 2009, Barr *et al.* (8) reported a novel "head-to-toe dimer" structure for the cytoplasmic D1D2 of PTPRG, in which D1 of one molecule interacted with D2 of the other molecule (counterpart) and vice versa. However, the authors stated that "future studies are necessary to establish this molecular mechanism *in vivo* as a form of inhibitory regulation."

PTPRZ is a member of the R5 RPTP subfamily together with PTPRG (3). Both molecules structurally resemble each other and contain a carbonic anhydrase (CAH)-like domain and fibronectin type III-like domain extracellularly as well as two tyrosine phosphatase domains intracellularly. Three splicing variants of PTPRZ are known: PTPRZ-A, a full-length receptor form; PTPRZ-B, a short receptor form with a deletion in the extracellular region; and PTPRZ-S (also called phosphacan), a secretory form (9). These receptor isoforms have been further subdivided into two subtypes; conventional PTPRZ-A and -B and exon 16-deleted PTPRZ-$A_{\Delta ex16}$ and -$B_{\Delta ex16}$, respectively (10).

All three isoforms expressed in the central nervous system are heavily modified with chondroitin sulfate chains on their extracellular segment (9). The chondroitin sulfate moiety is essential for the diffuse distribution of PTPRZ receptors on the cell membrane, thereby maintaining them in their catalytically active monomer state. Chondroitin sulfate chains are required for achieving the high-affinity binding sites of endogenous inhibitory ligands, such as pleiotrophin (PTN)/heparin-binding growth-associated molecule, midkine, basic fibroblast growth factor, and interleukin-34 (11). Positively charged ligands induce PTPRZ clustering, potentially by neutralizing electrostatic repulsion between negatively charged chondroitin sulfate chains, thereby inactivating the intracellular catalytic activities of PTPRZ receptors through dimerization in living cells (11). In contrast, PTPRG is not modified by chondroitin sulfate chains on the extracellular region, and no extracellular ligands have been identified to date.

PTPRZ is the most abundant RPTP molecule in oligodendrocyte precursor cells (OPCs) (12). It functions as a counterpart of FYN tyrosine kinase and dephosphorylates p190RhoGAP (13). The expression of PTPRZ-A, PTN, and myelin basic protein (MBP) peaks on postnatal day 5 (P5), P10, and P30, respectively, during development. On P10, the amounts of MBP and myelinated axons in the brain were shown to be significantly higher in *Ptprz*-null knockout mice than in WT animals (11). Conversely, *Ptn*-knockout mice exhibited delayed myelination (11). Consistent with these *in vivo* findings, oligodendrocytes appear earlier in primary cultures from *Ptprz*-deficient mice than from WT mice (12). In addition, PTN promotes thyroid hormone-induced OPC differentiation in glial cells obtained from WT mice, but not those from *Ptprz*-null knockout mice (12). These findings indicate that PTN-PTPRZ signaling fine-tunes the timing of oligodendrocyte differentiation and myelination in the developing mouse brain. However, there is currently no experimental evidence to show that the ligand-induced inactivation of RPTP molecules is performed by intracellular dimer formation or that it is relevant to physiological events.

In the present study, we show that the crystal structure of rat PTPRZ has the head-to-toe dimer configuration. The results obtained from several distinct methods, including native mass spectrometry (MS) and cell-based assays, support the validity of this inactivation mechanism in the ligand-induced inactivation of PTPRZ in living cells. Furthermore, primary cultured glial cells show its physiological relevance to the mechanisms responsible for OPC differentiation. Under "Discussion," we added overall considerations regarding the dimer interface region in RPTP family members.

Results

Crystal structures of tandem PTP domains of rat PTPRZ

We achieved the crystallization of the whole intracellular region of rat PTPRZ (rat PTPRZ-ICR) (see Fig. 1*A*) using the sitting-drop vapor-diffusion method, and solved the structure at 3.32 Å resolution (Fig. 1*B* and Table S1). The quality of the crystal structure was not so high that we could not discuss the structure in full detail; however, it was enough to conclude that PTPRZ-ICR takes the head-to-toe dimer formation (the PDB validation report is available (PDB code 6J6U), see also Table S1). Contact sites across the dimer interface are shown in Fig. 2*A*. This interaction involved extensive electrostatic interactions between a positively charged pocket at the active center of D1 in one molecule and a negatively charged surface between strands $\beta10-\beta11$ of D2 in the other molecule (see the *right panels* in Fig. 2*A*, *a* and *b*). The approximate area of the solvent-accessible interface between the two molecules was calculated to be 1230 $Å^2$ (5.1% of the total surface), and multiple hydrogen bonds and salt bridges were estimated using PDBePISA (Table S2), with two residues of Asp-2178 and Asp-2179 within the loop connecting strands $\beta10-\beta11$ in D2 exhibiting the most extensive interactions (Fig. 2*B*). These structural features are similar to those reported for the dimer structure of PTPRG-D1D2 (PDB code 2NLK) (8).

Masking the active site in D1 with D2 in response to ligand binding

Mass spectrometry (MS) under nondenaturing conditions, referred to as native MS, was used to investigate noncovalent molecular interactions in aqueous solution (14). Native MS revealed that PTPRZ-ICR proteins were in monomer-dimer equilibrium in solution, and dimers were observed in the concentrations higher than 3.2 μM, and the apparent K_d value was calculated to be 5.8 $\pm$ 1.54 μM (Fig. 3*A*). If the head-to-toe dimer configuration was present in solution as well as in the crystal structure, substrate binding may only take place in the monomer state. To test this possibility, we used a nonhydrolyzable pTyr mimetic (F_2Pmp, phosphono difluoromethyl phenylalanine)-containing peptide (15) based on the typical substrate motif for PTPRZ (16). The substrate mimetic, F_2Pmp-$GIT1_{550-556}$, effectively inhibited the catalytic activity of PTPRZ-ICR (K_i = 3.1 μM).[5] In native MS analyses, the competitive PTPRZ inhibitor, SCB4380 specifically bound to the monomer fraction of PTPRZ-ICR in a 1:1 stoichiometry, whereas no

[5] A. Fujikawa, K. Kuboyama, and M. Noda, unpublished data.

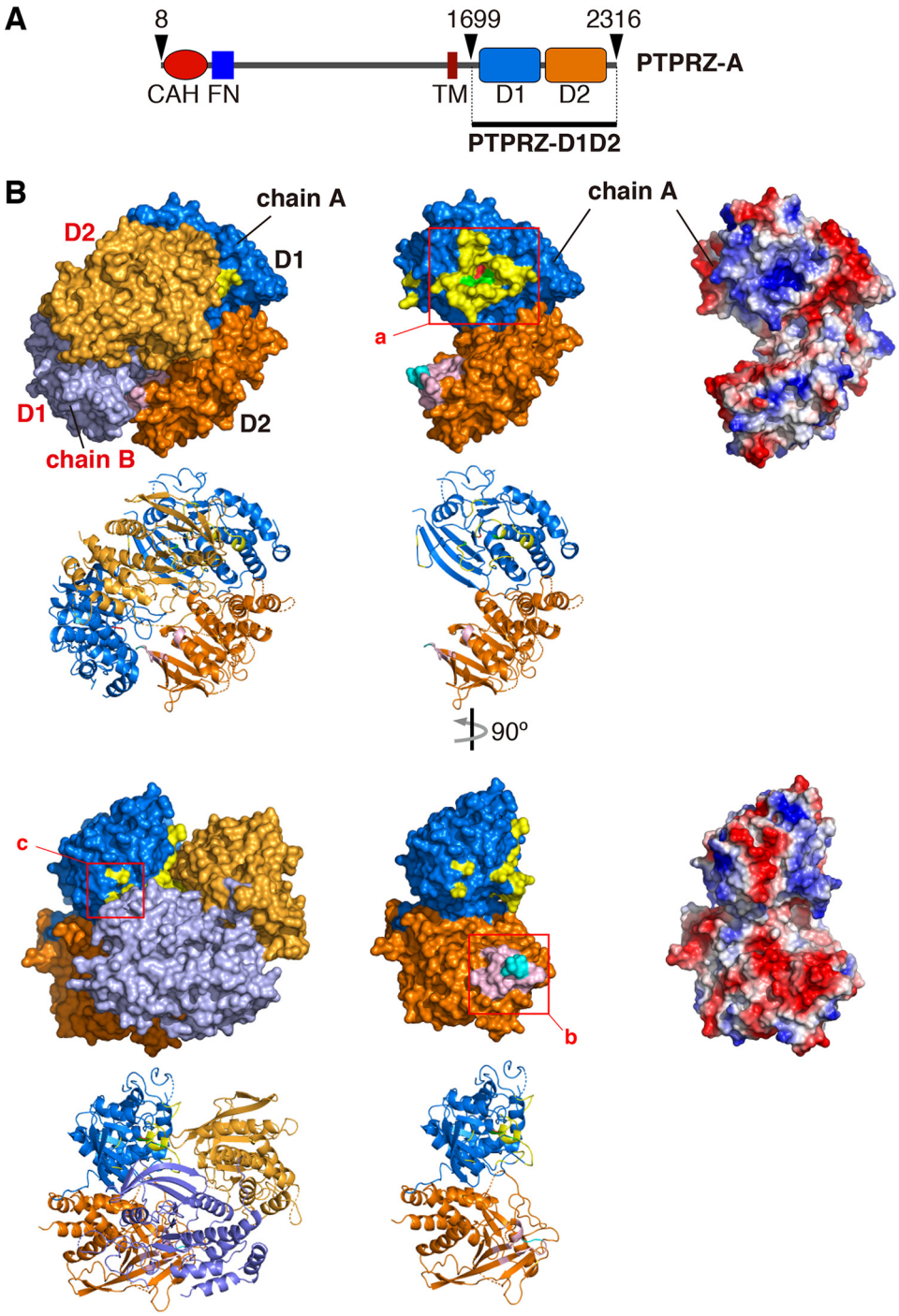

Figure 1. PTPRZ-ICR dimer structure. *A*, schematic diagram of rat PTPRZ-A receptor isoform. The region of PTPRZ-D1D2 (PTPRZ-ICR) is indicated by the *underline*. *CAH*, carbonic anhydrase-like domain; *FN*, a fibronectintype III domain; *TM*, transmembrane segment; *D1*/*D2*, intracellular PTP domains. *B*, surface and cartoon representations of rat PTPRZ-ICR (PDB 6J6U) in which the two molecules (chains A and B) formed a head-to-toe dimer, with the D1 domain (*blue* and *light purple*) of one molecule interacting with the D2 domain of a second molecule (*orange* and *yellow-orange*) (*left*). Chain A extracted from the dimer is shown by surface and cartoon representations (*center*) or electrostatic potentials colored *red* for a negative charge and *blue* for a positive charge (*right*). The three interface regions are indicated by *square boxes* (*a*–*c*), and their details are shown in Fig. 2*A*.

binding was observed in the dimer fraction (Fig. 3*B*). Similar results were obtained when mixed with F_2Pmp-GIT1$_{550-556}$ (Fig. 3*C*). Notably, increases in F_2Pmp-GIT1$_{550-556}$ or SCB4380-bound monomers inversely correlated with decreases in the dimer fraction. These results indicated that PTPRZ-ICR continuously shifts between monomer and dimer states, and that the substrate mimic prevents dimer formation when bound to the catalytic pocket in D1.

We then produced two PTPRZ-ICR mutant proteins: one (DDKK mutant) in which Asp-2178 and Asp-2179 (the residues are shown in *red letters* in Fig. 2*A*, *b*) were substituted with Lys residues to test its dimerization ability in solution; the other was the D2 domain-deleted form (ΔD2 mutant) to examine its blocking ability of the catalytic site of D1. ΔD2 and DDKK mutant enzymes exhibited similar PTPase activities, and their IC_{50} values for SCB4380 were similar to that of WT

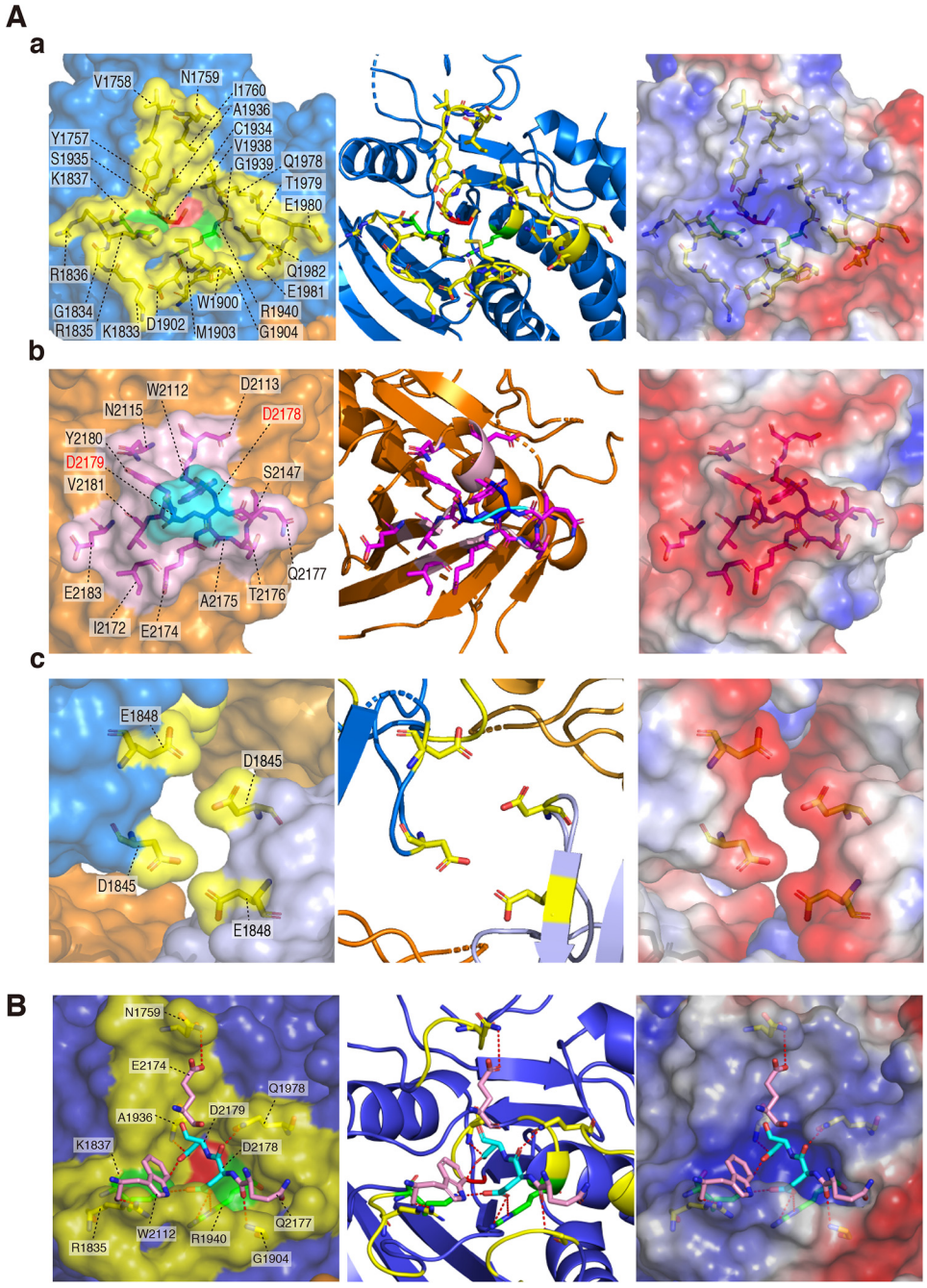

Figure 2. Dimer interface. *A, a-c*, amino acid residues forming the dimer interface are shown by a stick model inside the transparent surface (*left*), cartoon diagram (*middle*), and electrostatic potentials (*right*). Interface regions are colored as described in the legend to Fig. 1. Asp-2178 and Asp-2179 residues (shown in "*red*") were mutated to Lys residues in DDKK mutants. *B*, interactions between the D1 and D2 dimer interfaces are shown by *red dashed lines* (details are given in Table S1).

PTPRZ-ICR (Fig. S1). Both mutant proteins remained mostly as monomers within the concentrations tested and bound SCB4380 in a 1:1 stoichiometry in native MS (Fig. 4), indicating that SCB4380 did not bind to D2. These results strengthened our view that head-to-toe dimer formation underlies the ligand-induced inactivation of PTPRZ. These results were summarized in Fig. 5.

Role of D2 in ligand-induced PTPRZ inactivation

We transfected four constructs expressing the WT PTPRZ-B receptor isoform (WT), PTPase-inactive mutant PTPRZ-B (CS), D2-deleted PTPRZ-B (ΔD2), or Asp-2178/2179 to Lys mutant (DDKK) into BHK-21 cells, which do not endogenously express PTPRZ proteins (17), together with p190RhoGAP (p190), one of the PTRPZ substrates. Similar to WT PTPRZ-B, ΔD2 and DDKK mutants reduced the tyrosine phosphorylation levels of FLAG-tagged p190, a key signaling molecule in the OPC differentiation process (13), significantly more than the mock control or PTPase-inactive CS mutant (Fig. S2). These results indicated that ΔD2 and DDKK mutants were active PTPase in living cells. The tyrosine phosphorylation level of p190 expectedly increased in WT PTPRZ-B–

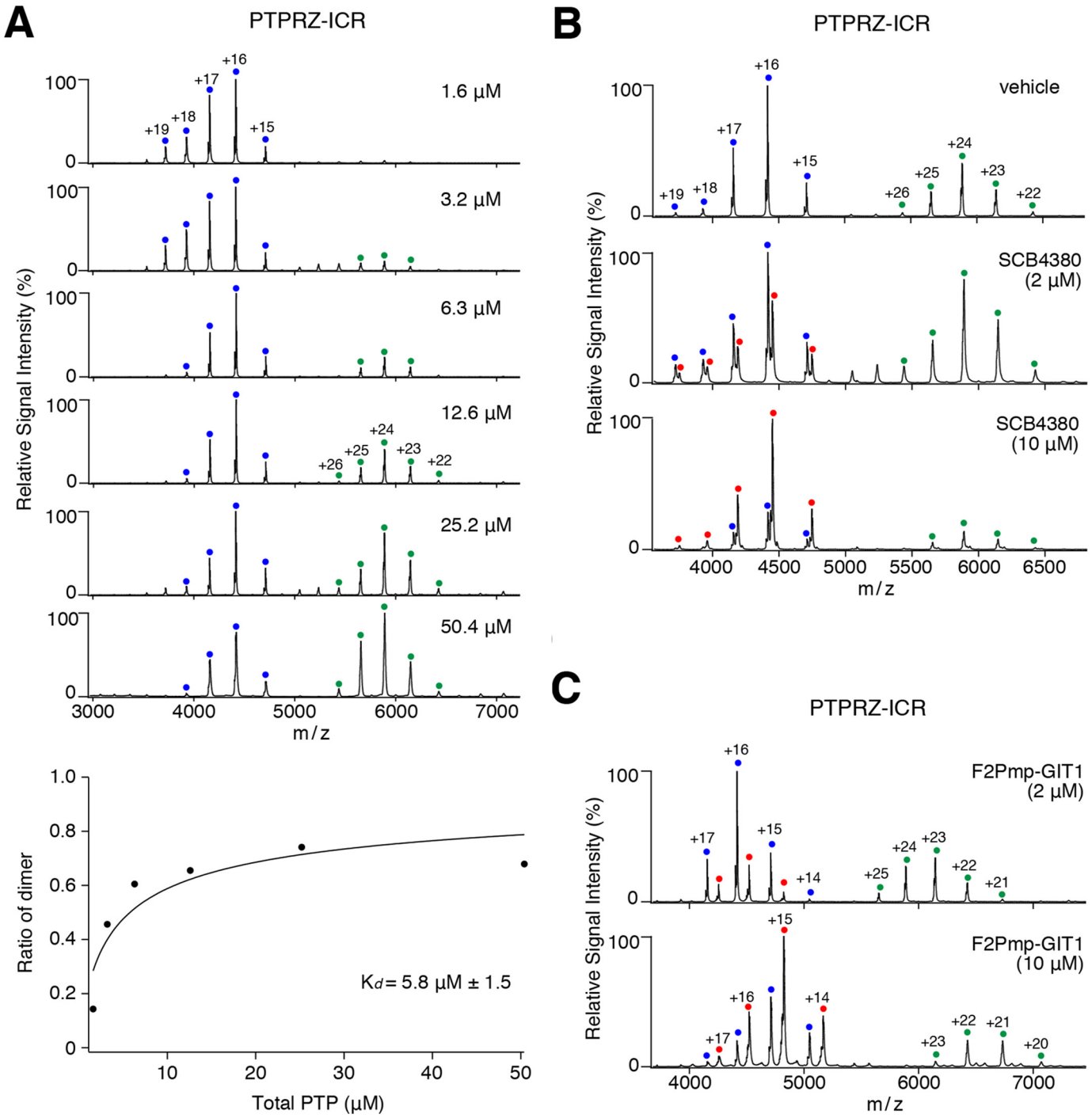

Figure 3. Native MS analyses for the monomer-dimer equilibrium of rat PTPRZ-ICR and inhibitor binding in aqueous solution. *A*, the monomer-dimer equilibrium of rat PTPRZ-ICR proteins at the indicated concentrations was assessed by MS under nondenaturing conditions. Product ion spectra derived from monomers (corresponding to a molecular mass of 70,639 ± 1 Da) or dimers (141,287 ± 8 Da) are indicated by *blue* and *green dots* with charge states, respectively. The concentration of dimer determined from the relative signal intensities in the mass spectrum was plotted as a function of increasing PTPRZ-ICR concentration at the *bottom* of the figure. The affinity was determined by curve fitting, and shown as the mean ± S.D. of three measurements. *B* and *C*, PTPRZ-ICR proteins (12.6 μM) were mixed with a small competitive inhibitor molecule, SCB4380 (*B*), or substrate-mimetic inhibitor peptide, F2Pmp-GIT1 (*C*), at the indicated concentrations, and then subjected to the MS analysis. Peaks corresponding to PTPRZ-ICR monomers complexed with SCB4380 (71,178 ± 2 Da) or F2Pmp-GIT1 (72,322 ± 1 Da) are indicated by *red dots* with charge states. MS peaks corresponding to PTPRZ-ICR dimers complexed with SCB4380 or F2Pmp-GIT1 were not observed. Masses were estimated from their parent ion peaks, and shown as the mean ± S.D. of three measurements.

expressing cells upon the PTN treatment, but not in the other transfectants expressing the CS, DDKK, or ΔD2 mutant, or mock control (Fig. 6*A*). When these cells were treated with the cell-permeable PTPRZ inhibitor NAZ2329, p190 phosphorylation levels increased in cells with PTPRZ-B, or its mutant ΔD2 or DDKK, but not in cells with the CS mutant or mock control (Fig. 6*B*). These results supported the view that ΔD2 and DDKK mutations in PTPRZ-B receptors eliminated PTN sensitivity to inactivate PTPase because of a deficiency in dimerization.

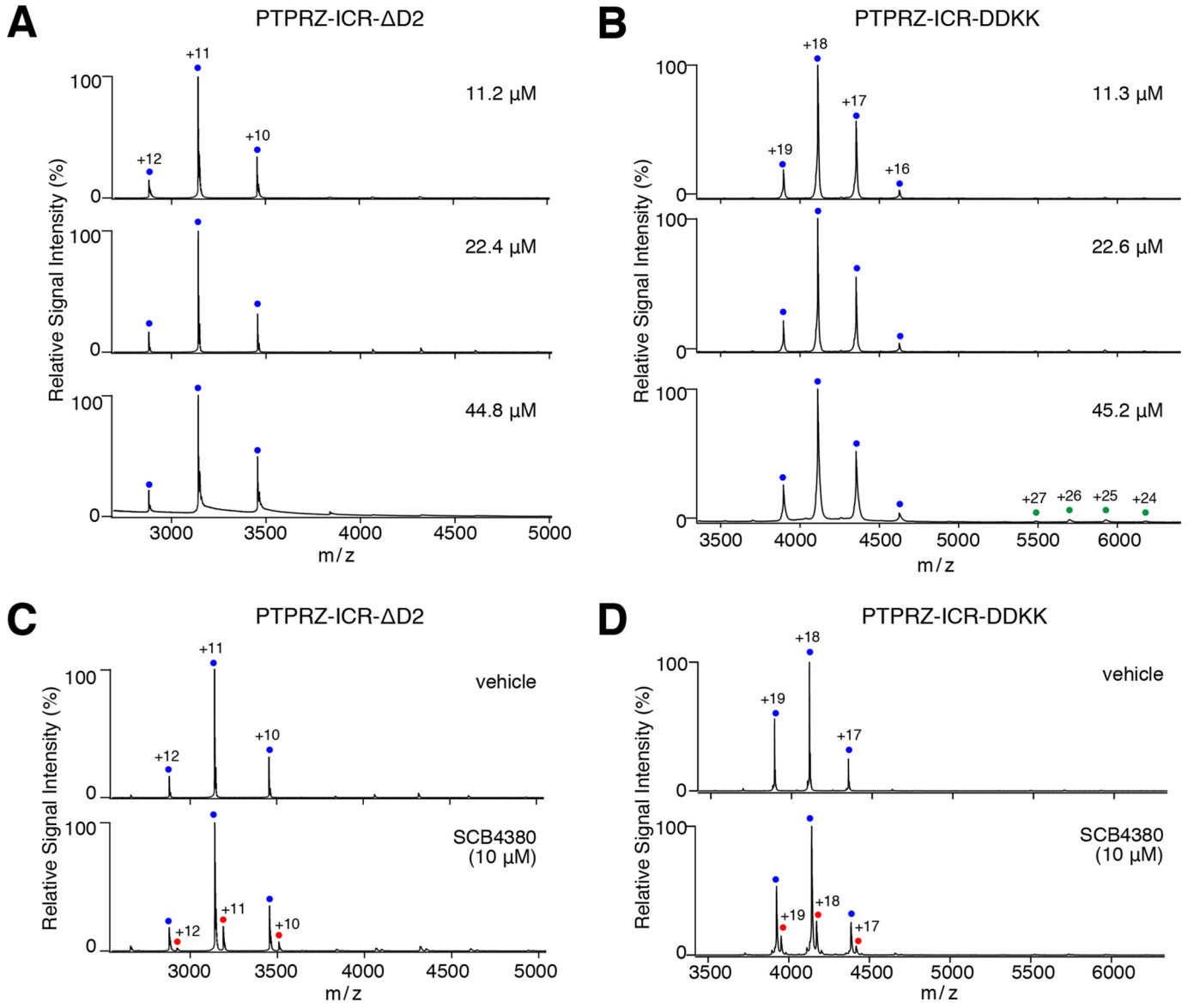

Figure 4. Monomer-dimer equilibrium of ΔD2 and DDKK mutants in aqueous solution. *A* and *B*, the monomer-dimer equilibrium of ΔD2 (*A*) and DDKK (*B*) mutants of PTPRZ-ICR was analyzed as described in the legend to Fig. 3*A*. Product ion spectra derived from the corresponding monomers (ΔD2, 34,543 ± 0 Da; DDKK, 73,979 ± 0 Da) are indicated by *blue dots* with charge states. Peaks corresponding to ΔD2 or DDKK dimers were not observed. *C* and *D*, ΔD2 (22.4 μM, *C*) and DDKK (22.6 μM, *D*) mutant proteins were mixed with SCB4380 at the indicated concentrations, and analyzed as described in the legend to Fig. 3*B*. Peaks corresponding to ΔD2 monomers complexed with SCB4380 (35,079 ± 9 Da) or DDKK monomers complexed with SCB4380 (74,523 ± 8 Da) are indicated by *red dots* with charge states. Masses were estimated from their parent ion peaks, and shown as the mean ± S.D. of three measurements.

After the PTN treatment, PTPRZ-B receptors exhibit a patchy distribution in contrast to their diffuse distribution on the cell surface (11, 17). The three mutants showed patchy distributions upon the PTN treatment as well as WT PTPRZ-B (compare *con* to *PTN* in Fig. 7), notwithstanding that their ICR proteins did not form a stable dimer *in vitro*. Of note, NAZ2329 treatment did not affect the cell surface distribution of PTPRZ-B or its mutant forms (Fig. 7). These results indicated that the PTPRZ receptor clustering itself is independent of its dimer formation or PTPase inactivation.

Effects of the ΔD2 mutation on PTN-enhanced OPC differentiation

To test its physiological significance, we performed a primary culture of neonatal mixed glial cells prepared from WT mice, *Ptprz*-knockout (KO) mice lacking all three PTPRZ isoforms (18), *Ptprz*-CS mutant knock-in mice (19), and ΔD2 mutant knock-in mice (20). The cell number ratios of MBP-positive mature oligodendrocytes relative to NG2-positive OPCs were similar between WT and ΔD2 knock-in glial cells under normal differentiation conditions (without PTN, *con* in Fig. 8, *A* and *B*). However, CS knock-in cells, as well as *Ptprz*-KO cells (13), showed higher differentiation levels than WT cells (Fig. 8, *A* and *B*), indicating that PTPase activity negatively regulated OPC differentiation. We already reported that PTN enhanced OPC differentiation to MBP-positive cells in WT cells, but not in *Ptprz*-KO cells (13), and herein demonstrated that neither CS nor ΔD2 knock-in cells responded to the PTN stimulation (Fig. 8*C*). On the other hand, NAZ2329 enhanced the differentiation of ΔD2 knock-in cells as well as WT cells (21), but not *Ptprz*-KO

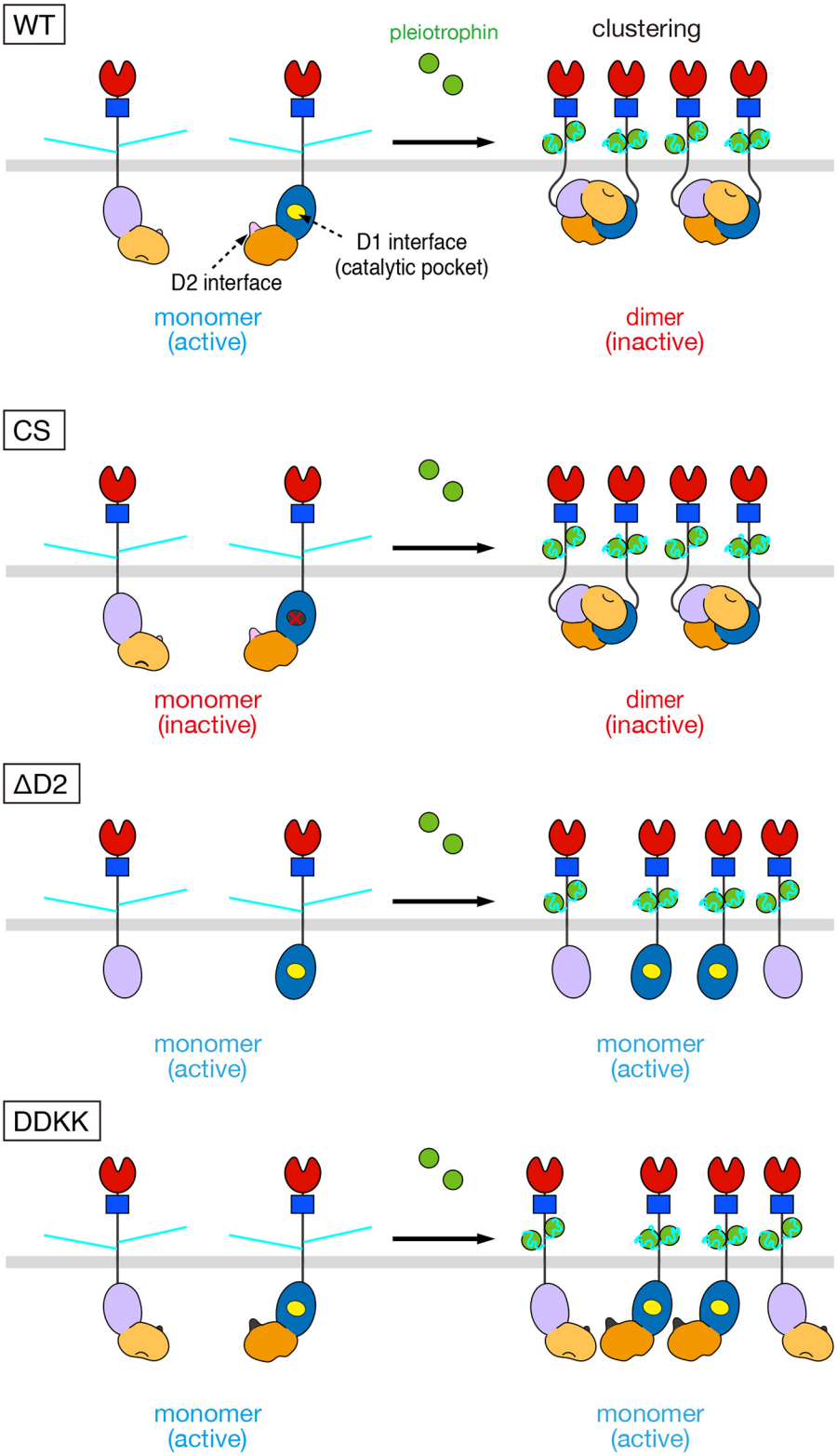

Figure 5. Models for ligand-induced clustering and dimerization for WT and mutant PTPRZ-B. PTPRZ-B receptors are expected to exist as monomers, but undergo clustering by extracellular ligand (*PTN*) binding, facilitating the head-to-toe dimer formation of the intracellular part, thereby masking the catalytic site of D1 by D2 from another (*WT*). On the other hand, the Cys-1930 to Ser mutation (*CS*) results in inactivation of the D1 domain but has no effects on the ligand-induced dimerization. The loss of the regulatory D2 domain (ΔD2) and the mutation in the dimer interface on D2 (DDKK) are catalytically active, but lacking the ligand-induced PTPase inactivation; however, ΔD2 and DDKK mutants are sensitive to PTPase inhibitors that bind to the active site. Domains are highlighted in different colors: carbonic anhydrase-like (*red*), fibronectin type III (FNIII, *blue*), PTP-D1 (*blue* or *light purple*), and PTP-D2 (*orange* or *yellow-orange*) domains. The extracellular regions of the three isoforms are highly glycosylated with chondroitin sulfate chains (*light blue lines*).

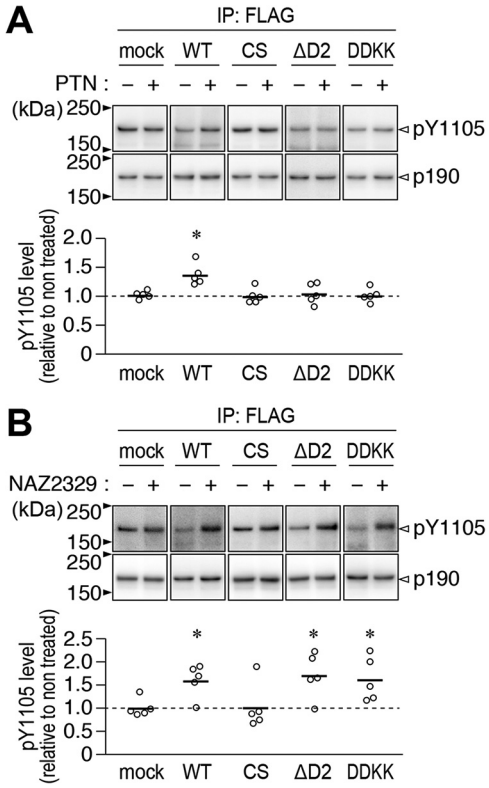

Figure 6. Effects of PTN and NAZ2329 on the tyrosine phosphorylation of p190RhoGAP in BHK-21 cells expressing PTPRZ or its mutant. *A* and *B*, BHK-21 cells were transfected with WT PTPRZ-B, its CS, ΔD2, or DDKK mutant, or the mock control, together with FLAG-tagged p190RhoGAP. Transfected cells were treated with 100 nM PTN or vehicle (*A*), or 25 μM NAZ2329 or vehicle (*B*) for 1 h. The Tyr-1105 phosphorylation of FLAG-tagged p190RhoGAP immunoprecipitation was assessed using anti-Tyr(P)-1105 and anti-FLAG antibodies, respectively. The scatter plot shows Tyr-1105 phosphorylation levels relative to vehicle-treated levels ($n = 5$ independent cell culture per group). *, $p < 0.05$; significantly different from the vehicle-treated control of each group by Welch's *t* test. Full-length blots for those that are cropped are shown in Fig. S4.

cells or CS knock-in cells. These results indicated that head-to-toe RPTP dimerization is relevant to OPC differentiation as the molecular basis for PTN-induced PTPRZ inactivation.

Discussion

PTP family members contain a common $CX_5R(S/T)$ sequence, in that the cysteine residue that performs the initial nucleophilic attack of phospho-Tyr in substrate proteins is sensitive to oxidation and inactivation by reactive oxygen species (22). This redox-dependent inactivation is reversible (23, 24), and is now widely recognized as a mechanism responsible for the down-regulation of PTPase activities in controlling signal outputs following an extracellular stimulus (22). On the other hand, the dimerization-induced inactivation of RPTP remains a controversial mechanism. The initial wedge model proposed from the crystal structure of PTPRZ-D1 is incompatible with the tandem PTP domain structures due to a steric clash with the D2 domain (7, 8). The head-to-toe dimer inactivation model was subsequently proposed from the crystal structure of the PTPRG-D1D2 segment, with D2 masking the catalytic site of D1 (8); however, its validity as the inhibitory regulation mechanism has not yet been investigated. The crystal structure of the D1D2 segment of PTPRZ also showed the head-to-toe dimer conformation (Figs. 1 and 2). Consistent with this structure, the inhibitory effects of PTN were abolished in living cells by the deletion or mutation of the regulatory D2 domain (Figs. 6 and 8), confirming its physiological relevance. To the best of our knowledge, the present study is the first to elucidate the molecular basis for the ligand-induced inactivation of PTPase *in vivo*.

Previous findings obtained from analytical ultracentrifugation for PTPRG indicated the concentration-dependent and stable dimerization of the D1D2 segment in solution with a K_d value of ~4 μM (8), which is close to the apparent K_d value of 5.8 μM for the dimer-monomer equilibrium of PTPRZ-ICR obtained from the native MS analysis (Fig. 3*A*). In addition, the competitive inhibitor, SCB4380 dose-dependently reduced dimer peaks (Fig. 3*B*). These results suggest that PTPRZ-ICR proteins exist in dynamic monomer-dimer equilibrium in solution. It is important to note the close proximity of Asp-1845 on one PTPRZ molecule and Glu-1848 on the other (Fig. 2*A*, *c*), which may cause charge repulsion and prevent stable dimer formation. The rapid association/dissociation of intracellular D1D2 may be a suitable property for a regulatory mechanism.

D2 truncation (ΔD2) abolished the dimerization abilities of PTPRZ-ICR proteins without changing SCB4380 binding abilities *in vitro* (Fig. 4). In living cells, the ΔD2 mutant receptors of PTPRZ-B exogenously expressed were not inactivated by PTN (Fig. 6), indicating a causal relationship between the masking effects of D2 on the catalytic site and ligand-induced PTPase inactivation. The results of PDBePISA showed multiple interactions in the dimer interface between D1 and D2 (Table S2). The interactions between acidic Asp-2178 and Asp-2179 residues in D2 and basic Lys-1837 and Arg-1940 residues in D1 are expected to be major stabilizing forces of the dimer structure. The substitution of Asp-2178 and Asp-2179 with Lys residues (DDKK mutant) largely abolished the dimerization abilities similar to the D2 deletion (Fig. 4). The DDKK substitution also disrupted the dimerization ability of PTPRG (8). Therefore, "head-to-toe dimerization" may be a conserved regulatory mechanism in two members of the R5 RPTP subfamily.

In contrast to the close similarities between the intracellular parts in PTPRZ and PTPRG, their extracellular regions display different characteristic features. The most obvious difference is the specific modification of PTPRZ with extensive glycosaminoglycans (9, 25), which is of crucial importance for the ligand-dependent regulation of PTPase inactivation (11). The negatively-charged chondroitin sulfate moiety is essential for the diffuse distribution of PTPRZ receptors at the cell membrane due to electrostatic repulsion, thereby maintaining them in a catalytically active monomer state (11). Notably, chondroitin sulfate chains are required for high-affinity ligand binding (26, 27). The accumulative binding of positively charged PTN attenuates electrostatic repulsion between chondroitin sulfate chains and induces the clustering of PTPRZ receptors (11), which may be a prerequisite for allowing the head-to-toe dimerization of intracellular parts in living cells (Figs. 6 and 8). On the other hand, these chondroitin sulfate modifications were not found in PTPRG (28), and no ligand molecules have been identified. Thus, regarding PTPRG, studies to confirm the *in vivo* relevance of this inhibitory regulation mechanism will be necessary in the future.

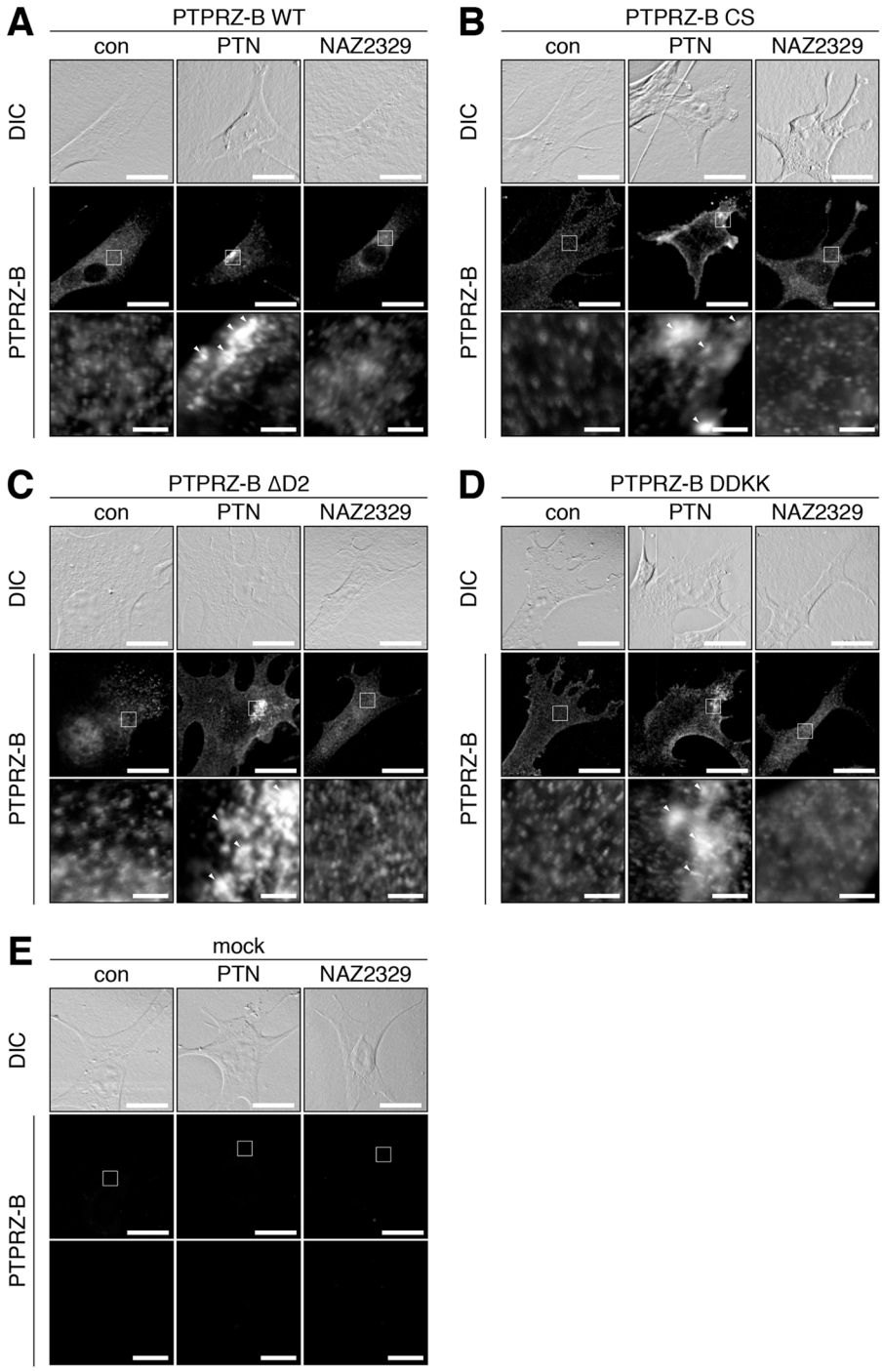

Figure 7. PTN-induced clustering of PTPRZ and its mutant in BHK-21 cells. *A–E*, BHK-21 cells were transfected with WT PTPRZ-B (*A*), CS (*B*), ΔD2 (*C*), or DDKK (*D*) mutant, or the mock control (*E*), and treated with PTN or NAZ2329, as described in the legend to Fig. 6. Cells were fixed with formalin and stained with anti-PTPRZ-S against the extracellular epitope of PTPRZ. The membrane permeabilization step was omitted to prevent antibody staining of the cytosol, as described previously (17). The *bottom* picture in each column is an enlarged view of the *rectangular region* in the *middle*. *Arrowheads*, anti-PTPRZ-S-positive puncta. *Scale bars*, 100 μm (*top* and *middle pictures*) and 10 μm (*bottom pictures*), respectively. *DIC*, differential interference contrast.

Barr *et al.* (8) also reported that the orientations of D1 and D2 of PTPRC, PTPRE, PTPRF, PTPRS, and PTPRG were highly conserved, suggesting that head-to-toe dimerization is a general regulatory mechanism for these RPTPs. Most of the residues involved in the dimer interface of the D1 side are well-conserved not only in tandem-type RPTP members, but also in all PTP family members, whereas key Asp–Asp residues on the D2 side of R5 members (PTPRZ and PTPRG) are changed to Arg–Lys in the R1/R6 member (PTPRC), Gln–Asp/Glu in R2B (PTPRK, PTPRM, PTPRT, and PTPRU), Asp–Gly in R2A members (PTPRD, PTPRF, and PTPRS), or Glu–Asn in a R4 member (PTPRA) (see Fig. S3). These changes may abolish or reduce dimer formation. As one exception, only PTPRE in the R4 subfamily contains acidic Glu–Glu residues as R5 RPTP members. However, dimer formation was not found in PTPRE-D1D2, similar to PTPRA, PTPRC, and PTPRM (8). Regarding

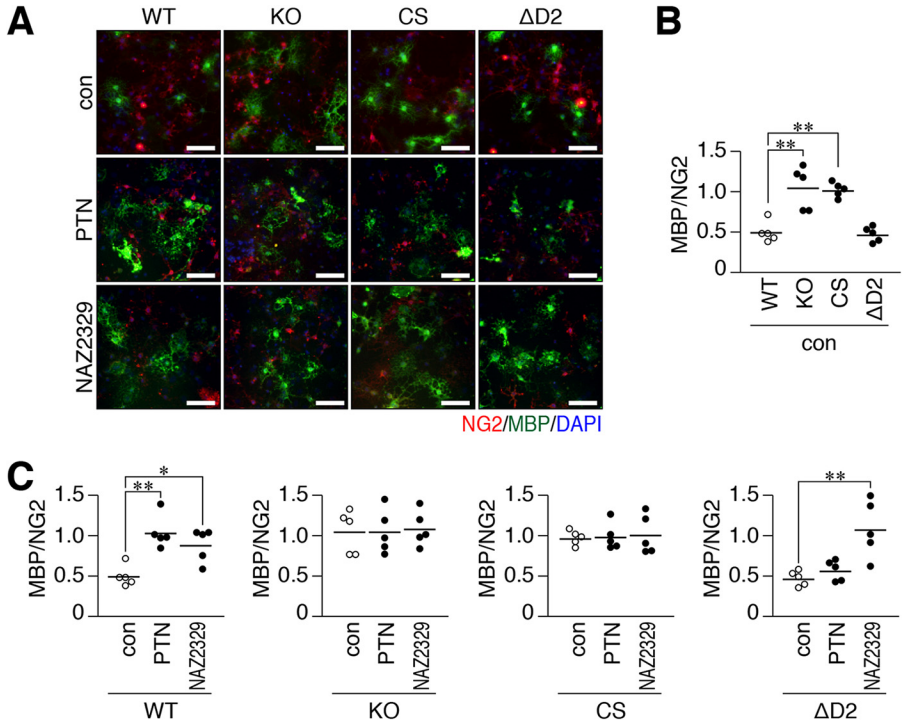

Figure 8. Effects of the *Ptprz*-CS or ΔD2 knock-in mutation on the PTN- or NAZ2329-stimulated differentiation of oligodendrocyte precursors cells into mature oligodendrocytes. *A–C*, glial cells were prepared from WT, KO, CS, or ΔD2 brains and cultured in differentiation medium in the presence of 100 nM PTN, 25 μM NAZ2329, or vehicle for 6 days. Fixed and permeabilized cells were stained with anti-NG2 proteoglycan (a marker of oligodendrocyte precursor cells, OPCs; *red*) and anti-MBP (oligodendrocytes, *green*) antibodies in conjunction with the DAPI labeling of nuclei (*blue*) (*A*). *Scale bars*, 100 μm. Scatter plots show the ratio of MBP-positive cells to NG2-positive cells, in which each *circle* corresponds to an independent cell culture ($n = 5$ each). *, $p < 0.05$; **, $p < 0.01$, significantly different from WT cells under control conditions (*B*), or the vehicle control of each group (*C*) by analysis of variance with Bonferroni's post hoc tests.

R4 members, acidic Glu residue(s) are adjacent to conserved Lys (corresponding to Lys-1837 of rat PTPRZ) on the D1 side, which may interfere with dimerization.

Besides homodimerization, the heterodimerization of RPTP family members may be possible *in vivo*. In support of this view, the D2 domains of PTPRZ, PTPRA, and PTPRM were isolated in a yeast two-hybrid screen as interactors of the cytoplasmic region of PTPRZ (29). The dimerization of RPTPs may also be regulated by post-translational modifications, such as oxidation (22, 30, 31). The involvement of these factors in head-to-toe dimerization needs to be investigated in future studies.

Experimental procedures

Ethics statement and experimental animals

All animal experimental protocols used in the present study were approved by the Institutional Animal Care and Use Committee of National Institutes of Natural Sciences, Japan (approval number 17A020). Mouse pups were handled gently to minimize stress and quickly decapitated without anesthesia, and brains were collected. *Ptprz*-null knockout mice (18), *Ptprz*-ΔD2– knock-in mice (20), and *Ptprz*-CS– knock-in mice (19) were backcrossed with the inbred C57BL/6J strain (CLEA Japan) (WT) for more than 10 generations.

Reagents and antibodies

SCB4380 (32), NAZ2329 (21), and recombinant PTN (33) were described previously. Stock solutions of PTN were prepared as 100 μg/ml with PBS (4.3 mM Na_2HPO_4, 1.4 mM KH_2PO_4, 137 mM NaCl, and 2.7 mM KCl, pH 7.4) containing 100 μg/ml of BSA and stored at −85 °C until used. Anti-PTPRZ-S, rabbit polyclonal antibodies against the extracellular region of PTPRZ (34), and anti-pY1105, purified rabbit polyclonal antibodies against phosphorylated Tyr-1105 of p190RhoGAP (35), were described previously. The following are the specificities and sources of the commercially available antibodies used in the present study: anti-myelin basic protein (catalogue number sc-13914, Santa Cruz Biotechnology), anti-NG2 proteoglycan (catalogue number AB5320, Millipore), anti-p190RhoGAP (catalogue number 610150, BD Biosciences; and catalogue number 12164, Cell Signaling Technology), anti-phosphotyrosine (PY20; catalogue number ab16389, Abcam), and anti-FLAG (catalogue number F7425 for Western blotting and number F3165 for immunoprecipitation; Sigma).

X-ray crystallography of rat PTPRZ-D1D2

Recombinant proteins of rat PTPRZ-D1D2 (residues 1699–2316) were expressed using a baculovirus-silkworm expression system, and purified as described (32). The initial screening of crystallization conditions was performed using PACT (Molecular Dimensions). Crystals were obtained at 277 K in 14% (*w/v*) PEG3350, 200 mM potassium fluoride, and 0.1 M bistris propane, pH 6.5, by the sitting-drop vapor diffusion method. After a brief soaking in 14% PEG3350, 3.6 M potassium fluoride, and 0.1 M bistris propane, pH 6.5, crystals were flash-frozen in a cold nitrogen stream at 100 K. X-ray diffraction data were collected using an RAXIS IV^{2+} imaging-plate area detector mounted on a Rigaku MicroMax-007 rotating-anode source with CuKα radiation (λ = 1.5418 Å, 40 kV, 20 mA). Two hundred diffrac-

tion images were taken with a 1.0° oscillation. Diffraction data were processed and scaled with HKL2000 (36). The crystal structure was solved by the molecular replacement method using the structure of the D1 domain of PTPRZ (PDB code 5AWX) and the D1-D2 domain of PTPRG (PDB code 2NLK). A molecular replacement calculation was performed using AMoRe (37). The structural model was manually fit using Coot (38) and refined with Refmac-5 with local NCS restraints (39). Interface areas and interactions were calculated by "Protein interfaces, surfaces and assemblies" service PISA (40) at the European Bioinformatics Institute. Figures were created using PyMOL (DeLano Scientific).

Mass spectrometry under nondenaturing conditions and data analysis

Purified PTPRZ-D1D2 (32), PTPRZ-ΔD2 (residues 1699–1997), and PTPRZ-D1D2-DDKK mutant proteins expressed using the baculovirus-silkworm expression system were buffer exchanged to 100 mM ammonium acetate, pH 7.0, by passing through a MicroBioSpin-6 column (Bio-Rad), diluted 100-fold with the same buffer, and then kept on ice. Ten-microliter aliquots were mixed with equal volumes of individual fining compound solutions, and samples (~2 μl for each analysis) were immediately analyzed by nanoflow electrospray using in-house gold-coated glass capillaries. Spectra were recorded on a SYNAPT G2-Si HDMS mass spectrometer (Waters) in the positive ionization mode at 1.36 kV with 150 V of a sampling cone voltage and source offset voltage, 0 V of trap and transfer collision energy, and 2 ml/min trap gas flow. Spectra were calibrated using 1 mg/ml of cesium iodide and analyzed by MassLynx software (Waters).

To evaluate the value of the dissociation constant (K_D) between monomer and dimer forms, it was assumed that the monomer and dimer forms have similar detection efficiencies, and peak intensities are proportional to molar concentrations. The ratio of dimer to monomer was plotted *versus* the initial protein concentration and the K_D value was determined by curve fitting using the IGOR program (Wave Metrics).

Expression plasmids

The mammalian expression plasmids, pZeoPTPζ (for PTPRZ-B) (41) and pFLAG-p190 (for FLAG-tagged p190RhoGAP), were described previously (42), and pZeoPTPζ-ΔD2 (the D2 deletion mutant of PTPRZ-B) was generated using pZeoPTPζ as a template with a QuikChange multisite-directed mutagenesis kit (Stratagene).

BHK-21 cell culture and DNA transfection

Hamster kidney BHK-21 cells have been maintained in our laboratory. BHK-21 cells were cultured in DMEM (Life Technologies) supplemented with 10% fetal bovine serum (Nichirei Biosciences) in a humidified incubator at 37 °C with 5% CO_2. DNA transfection was performed using Lipofectamine 2000 reagent (Thermo Fisher Scientific) according to the manufacturer's directions.

Primary mixed glial culture

A primary mixed glial cell culture was performed as described previously (13). Cortex tissues obtained from mouse brains on postnatal day 1 were dissociated with papain (Worthington Biochemical). Dissociated cells (2.0×10^4 cells) were cultured on a poly-L-ornithine–coated 35-mm dish with DMEM differentiation medium mixed 1:1 (v/v) with Ham's F-12 (DMEM/F-12, Life Technologies), 1× GlutaMAX (Life Technologies), 1× N2 supplement (Life Technologies), 10 μg/ml of the AA homodimeric form of platelet-derived growth factor (PDGF-AA, Wako Pure Chemical), 0.5% fetal bovine serum, 100 μg/ml of bovine serum albumin (BSA, Sigma), 10 nM biotin (Sigma), and 30 ng/ml of thyronine/thyroxine (Sigma) in a humidified incubator at 37 °C with 5% CO_2. On the sixth day of culture, cells were fixed and stained with anti-NG2 (a specific marker for OPCs) and anti-MBP (a marker for matured oligodendrocytes). Differentiation from OPC to oligodendrocytes was estimated from the ratio of MBP-positive cells to NG2-positive cells.

Immunocytofluorescence staining

Cells were fixed with 4% paraformaldehyde in PBS for 30 min. Fixed cells were permeabilized and blocked with 4% nonfat dry milk and 0.1% Triton X-100 in TBS (10 mM Tris-HCl, pH 7.4, 150 mM NaCl) for 30 min, and then incubated overnight with the respective primary antibodies at 4 °C. When cell-surface proteins were analyzed, the membrane permeabilization step was omitted to prevent antibody staining of the cytosol, as described previously (17). Bound primary antibodies were visualized with Alexa Fluor-conjugated secondary antibodies (Life Technologies) or DyLight Amine Reactive Dyes (DyLight 488 NHS Ester, Thermo Fisher Scientific) according to the standard procedure. Digital photomicrographs of individual specimens were taken with the Biozero BZ-8000 (Keyence), or LSM 700 confocal microscope (Zeiss).

Protein extraction and chABC digestion

Proteins were extracted from mouse brains or cultured cells with 1% Nonidet P-40 in TBS containing 1 mM vanadate, 10 mM NaF, and protease inhibitors (EDTA-free complete, Roche Molecular Biochemicals). Regarding the detection of PTPRZ proteins, tissue extracts with 1% Nonidet P-40 in TBS containing protease inhibitors (Complete, Roche Molecular Biochemicals) were mixed with an equal volume of 0.2 M Tris-HCl, 60 mM sodium acetate, 10 mM EDTA, pH 7.5, containing 25 microunits/μl of chABC (Sigma), or not (control), at 37 °C for 1 h.

Immunoprecipitation and Western blotting

Protein extracts were precleaned with Protein G-Sepharose (GE Healthcare) and subjected to immunoprecipitation with a combination of anti-FLAG M2 and Protein G-Sepharose beads. Immunocomplexes were then separated by SDS-PAGE, followed by semi-dry electroblotting onto a polyvinylidene difluoride membrane. After blocking with 4% nonfat dry milk and 0.1% Triton X-100 in TBS, membranes were incubated overnight with the respective antibodies. The binding of antibodies was detected with Luminata Forte Western HRP Substrate (Millipore). Regarding the detection of tyrosine-phosphorylated proteins in Western blotting, antibodies (PY20 or anti-

pY1105) were diluted with blocking solution (1% BSA and 0.1% Triton X-100 in TBS).

Image and statistical analyses

Quantitative image analyses were performed using ImageJ software (NIH) or Adobe Photoshop CS6 software (Adobe Systems). Statistical analyses were performed using IBM SPSS Statistics 25 software (IBM).

Author contributions—A. F., K. K., and M. N. funding acquisition; A. F., H. S., N. T., K. I., K. K., and R. S. investigation; A. F. methodology; A. F. writing-original draft; A. F. and M. N. project administration; H. S. and S. U. data curation; H. S., N. T., K. I., K. K., and S. U. formal analysis; H. S., K. I., and S. U. validation; H. S., K. I., and S. U. visualization; M. N. conceptualization; M. N. supervision; M. N. writing-review and editing.

Acknowledgments—We thank Yoshiko Isoshima and Norie Nakanishi for technical assistance, and Akiko Kodama for secretarial assistance. Immunofluorescence photomicrograph images were acquired at the Spectrography and Bioimaging Facility, NIBB Core Research Facilities. Native MS experiments were supported by the Joint Research by Exploratory Research Center on Life and Living Systems (ExCELLS).

References

1. Tonks, N. K. (2013) Protein tyrosine phosphatases: from housekeeping enzymes to master regulators of signal transduction. *FEBS J.* **280,** 346–378 CrossRef Medline
2. Schlessinger, J. (2002) Ligand-induced, receptor-mediated dimerization and activation of EGF receptor. *Cell* **110,** 669–672 CrossRef Medline
3. Andersen, J. N., Mortensen, O. H., Peters, G. H., Drake, P. G., Iversen, L. F., Olsen, O. H., Jansen, P. G., Andersen, H. S., Tonks, N. K., and Møller, N. P. (2001) Structural and evolutionary relationships among protein tyrosine phosphatase domains. *Mol. Cell. Biol.* **21,** 7117–7136 CrossRef Medline
4. Jiang, G., den Hertog, J., Su, J., Noel, J., Sap, J., and Hunter, T. (1999) Dimerization inhibits the activity of receptor-like protein-tyrosine phosphatase-α. *Nature* **401,** 606–610 CrossRef Medline
5. Bilwes, A. M., den Hertog, J., Hunter, T., and Noel, J. P. (1996) Structural basis for inhibition of receptor protein-tyrosine phosphatase-α by dimerization. *Nature* **382,** 555–559 CrossRef Medline
6. Nam, H. J., Poy, F., Krueger, N. X., Saito, H., and Frederick, C. A. (1999) Crystal structure of the tandem phosphatase domains of RPTP LAR. *Cell* **97,** 449–457 CrossRef Medline
7. Nam, H. J., Poy, F., Saito, H., and Frederick, C. A. (2005) Structural basis for the function and regulation of the receptor protein tyrosine phosphatase CD45. *J. Exp. Med.* **201,** 441–452 CrossRef Medline
8. Barr, A. J., Ugochukwu, E., Lee, W. H., King, O. N., Filippakopoulos, P., Alfano, I., Savitsky, P., Burgess-Brown, N. A., Müller, S., and Knapp, S. (2009) Large-scale structural analysis of the classical human protein tyrosine phosphatome. *Cell* **136,** 352–363 CrossRef Medline
9. Chow, J. P., Fujikawa, A., Shimizu, H., Suzuki, R., and Noda, M. (2008) Metalloproteinase- and γ-secretase-mediated cleavage of protein-tyrosine phosphatase receptor type Z. *J. Biol. Chem.* **283,** 30879–30889 CrossRef Medline
10. Fujikawa, A., Chow, J. P. H., Matsumoto, M., Suzuki, R., Kuboyama, K., Yamamoto, N., and Noda, M. (2017) Identification of novel splicing variants of protein tyrosine phosphatase receptor type Z. *J. Biochem.* **162,** 381–390 CrossRef Medline
11. Kuboyama, K., Fujikawa, A., Suzuki, R., Tanga, N., and Noda, M. (2016) Role of chondroitin sulfate (CS) modification in the regulation of protein-tyrosine phosphatase receptor type Z (PTPRZ) activity: pleiotrophin-PTPRZ a signaling is involved in oligodendrocyte differentiation. *J. Biol. Chem.* **291,** 18117–18128 CrossRef Medline
12. Kuboyama, K., Fujikawa, A., Suzuki, R., and Noda, M. (2015) Inactivation of protein tyrosine phosphatase receptor type Z by pleiotrophin promotes remyelination through activation of differentiation of oligodendrocyte precursor cells. *J. Neurosci.* **35,** 12162–12171 CrossRef Medline
13. Kuboyama, K., Fujikawa, A., Masumura, M., Suzuki, R., Matsumoto, M., and Noda, M. (2012) Protein tyrosine phosphatase receptor type Z negatively regulates oligodendrocyte differentiation and myelination. *Plos One* **7,** e48797 CrossRef Medline
14. Ishii, K., Zhou, M., and Uchiyama, S. (2018) Native mass spectrometry for understanding dynamic protein complex. *Biochim. Biophys. Acta* **1862,** 275–286 CrossRef
15. Burke, T. R., Jr., Kole, H. K., and Roller, P. P. (1994) Potent inhibition of insulin receptor dephosphorylation by a hexamer peptide containing the phosphotyrosyl mimetic F2Pmp. *Biochem. Biophys. Res. Commun.* **204,** 129–134 CrossRef Medline
16. Fujikawa, A., Fukada, M., Makioka, Y., Suzuki, R., Chow, J. P., Matsumoto, M., and Noda, M. (2011) Consensus substrate sequence for protein-tyrosine phosphatase receptor type Z. *J. Biol. Chem.* **286,** 37137–37146 CrossRef Medline
17. Fukada, M., Fujikawa, A., Chow, J. P., Ikematsu, S., Sakuma, S., and Noda, M. (2006) Protein tyrosine phosphatase receptor type Z is inactivated by ligand-induced oligomerization. *FEBS Lett.* **580,** 4051–4056 CrossRef Medline
18. Shintani, T., Watanabe, E., Maeda, N., and Noda, M. (1998) Neurons as well as astrocytes express proteoglycan-type protein tyrosine phosphatase ζ/RPTPβ: analysis of mice in which the PTPζ/RPTPβ gene was replaced with the *LacZ* gene. *Neurosci. Lett.* **247,** 135–138 CrossRef Medline
19. Tanga, N., Kuboyama, K., Kishimoto, A., Kiyonari, H., Shiraishi, A., Suzuki, R., Watanabe, T., Fujikawa, A., and Noda, M. (2019) The PTN-PTPRZ signal activates the AFAP1L2-dependent PI3K-AKT pathway for oligodendrocyte differentiation: targeted inactivation of PTPRZ activity in mice. *Glia* **67,** 967–984 CrossRef Medline
20. Tanga, N., Kuboyama, K., Kishimoto, A., Kihara, M., Kiyonari, H., Watanabe, T., Fujikawa, A., and Noda, M. J. (2019) Behavioral and neurological analyses of adult mice carrying null and distinct loss-of-receptor function mutations in protein tyrosine phosphatase receptor type Z (PTPRZ). *PLoS One* **14,** e0217880 Medline
21. Fujikawa, A., Sugawara, H., Tanaka, T., Matsumoto, M., Kuboyama, K., Suzuki, R., Tanga, N., Ogata, A., Masumura, M., and Noda, M. (2017) Targeting PTPRZ inhibits stem cell-like properties and tumorigenicity in glioblastoma cells. *Sci. Rep.* **7,** 5609 CrossRef Medline
22. Tonks, N. K. (2005) Redox redux: revisiting PTPs and the control of cell signaling. *Cell* **121,** 667–670 CrossRef Medline
23. Salmeen, A., Andersen, J. N., Myers, M. P., Meng, T. C., Hinks, J. A., Tonks, N. K., and Barford, D. (2003) Redox regulation of protein tyrosine phosphatase 1B involves a sulphenyl-amide intermediate. *Nature* **423,** 769–773 CrossRef Medline
24. van Montfort, R. L., Congreve, M., Tisi, D., Carr, R., and Jhoti, H. (2003) Oxidation state of the active-site cysteine in protein tyrosine phosphatase 1B. *Nature* **423,** 773–777 CrossRef Medline
25. Nishiwaki, T., Maeda, N., and Noda, M. (1998) Characterization and developmental regulation of proteoglycan-type protein tyrosine phosphatase ζ/RPTPβ isoforms. *J. Biochem.* **123,** 458–467 CrossRef Medline
26. Maeda, N., Nishiwaki, T., Shintani, T., Hamanaka, H., and Noda, M. (1996) 6B4 proteoglycan/phosphacan, an extracellular variant of receptor-like protein-tyrosine phosphatase ζ/RPTPβ, binds pleiotrophin/heparin-binding growth-associated molecule (HB-GAM). *J. Biol. Chem.* **271,** 21446–21452 CrossRef Medline
27. Maeda, N., Ichihara-Tanaka, K., Kimura, T., Kadomatsu, K., Muramatsu, T., and Noda, M. (1999) A receptor-like protein-tyrosine phosphatase PTPζ/RPTPβ binds a heparin-binding growth factor midkine: involvement of arginine 78 of midkine in the high affinity binding to PTPζ. *J. Biol. Chem.* **274,** 12474–12479 CrossRef Medline
28. Shintani, T., Maeda, N., Nishiwaki, T., and Noda, M. (1997) Characterization of rat receptor-like protein tyrosine phosphatase γ isoforms. *Biochem. Biophys. Res. Commun.* **230,** 419–425 CrossRef Medline
29. Adamsky, K., Arnold, K., Sabanay, H., and Peles, E. (2003) Junctional protein MAGI-3 interacts with receptor tyrosine phosphatase β (RPTPβ) and

tyrosine-phosphorylated proteins. *J. Cell Sci.* **116,** 1279–1289 CrossRef Medline
30. Blanchetot, C., Tertoolen, L. G., and den Hertog, J. (2002) Regulation of receptor protein-tyrosine phosphatase α by oxidative stress. *EMBO J.* **21,** 493–503 CrossRef Medline
31. Groen, A., Overvoorde, J., van der Wijk, T., and den Hertog, J. (2008) Redox regulation of dimerization of the receptor protein-tyrosine phosphatases RPTPα, LAR, RPTPμ, and CD45. *FEBS J.* **275,** 2597–2604 CrossRef Medline
32. Fujikawa, A., Nagahira, A., Sugawara, H., Ishii, K., Imajo, S., Matsumoto, M., Kuboyama, K., Suzuki, R., Tanga, N., Noda, M., Uchiyama, S., Tomoo, T., Ogata, A., Masumura, M., and Noda, M. (2016) Small-molecule inhibition of PTPRZ reduces tumor growth in a rat model of glioblastoma. *Sci. Rep.* **6,** 20473 CrossRef Medline
33. Murasugi, A., Kido, I., Kumai, H., and Asami, Y. (2003) Efficient production of recombinant human pleiotrophin in yeast, *Pichia pastoris*. *Biosci. Biotechnol. Biochem.* **67,** 2288–2290 CrossRef Medline
34. Chow, J. P., Fujikawa, A., Shimizu, H., and Noda, M. (2008) Plasmin-mediated processing of protein tyrosine phosphatase receptor type Z in the mouse brain. *Neurosci. Lett.* **442,** 208–212 CrossRef Medline
35. Tamura, H., Fukada, M., Fujikawa, A., and Noda, M. (2006) Protein tyrosine phosphatase receptor type Z is involved in hippocampus-dependent memory formation through dephosphorylation at Y1105 on p190 RhoGAP. *Neurosci. Lett.* **399,** 33–38 CrossRef Medline
36. Otwinowski, Z., and Minor, W. (1997) Processing of X-ray diffraction data collected in oscillation mode. *Methods Enzymol.* **276,** 307–326 CrossRef Medline
37. Navaza, J., and Saludjian, P. (1997) AMoRe: an automated molecular replacement program package. *Methods Enzymol.* **276,** 581–594 CrossRef Medline
38. Emsley, P., Lohkamp, B., Scott, W. G., and Cowtan, K. (2010) Features and development of Coot. *Acta Crystallogr. D Biol. Crystallogr.* **66,** 486–501 CrossRef Medline
39. Banks, J. L., Beard, H. S., Cao, Y., Cho, A. E., Damm, W., Farid, R., Felts, A. K., Halgren, T. A., Mainz, D. T., Maple, J. R., Murphy, R., Philipp, D. M., Repasky, M. P., Zhang, L. Y., Berne, B. J., Friesner, R. A., Gallicchio, E., and Levy, R. M. (2005) Integrated modeling program, applied chemical theory (IMPACT). *J. Comput. Chem.* **26,** 1752–1780 CrossRef Medline
40. Krissinel, E., and Henrick, K. (2007) Inference of macromolecular assemblies from crystalline state. *J. Mol. Biol.* **372,** 774–797 CrossRef Medline
41. Kawachi, H., Fujikawa, A., Maeda, N., and Noda, M. (2001) Identification of GIT1/Cat-1 as a substrate molecule of protein tyrosine phosphatase ζ/β by the yeast substrate-trapping system. *Proc. Natl. Acad. Sci. U.S.A.* **98,** 6593–6598 CrossRef Medline
42. Fukada, M., Kawachi, H., Fujikawa, A., and Noda, M. (2005) Yeast substrate-trapping system for isolating substrates of protein tyrosine phosphatases: Isolation of substrates for protein tyrosine phosphatase receptor type Z. *Methods* **35,** 54–63 CrossRef Medline